Journal of Inorganic Biochemistry 256 (2024) 112545

Contents lists available at ScienceDirect

Journal of Inorganic Biochemistry

journal homepage: www.elsevier.com/locate/jinorgbio

Trinuclear ruthenium(II) polypyridyl complexes: Evaluation as photosensitizers for enhanced cervical cancer treatment

Athi Welsh [a], Refilwe Matshitse [b], Saif F. Khan [c], Tebello Nyokong [b], Sharon Prince [c], Gregory S. Smith [a,*]

[a] Department of Chemistry, University of Cape Town, Rondebosch 7700, ,South Africa
[b] Institute for Nanotechnology Innovation, Rhodes University, Makhanda 6140, South Africa
[c] Division of Cell Biology, Department of Human Biology, University of Cape Town, Faculty of Health Science, Observatory, 7925, South Africa

ARTICLE INFO

Keywords:
Polynuclear
Benzimidazole
Ruthenium(II)
Anticancer
Photodynamic therapy

ABSTRACT

Trinuclear ruthenium(II) polypyridyl complexes anchored to benzimidazole-triazine / trisamine scaffolds were investigated as photosensitizers for photodynamic therapy. The trinuclear complexes were noted to produce a significant amount of singlet oxygen in both DMF and aqueous media, are photostable and show appreciable emission quantum yields (ϕ_{em}). In our experimental setting, despite the moderate phototoxic activity in the HeLa cervical cancer cell line, the phototoxic indices (PI) of the trinuclear complexes are superior relative to the PIs of a clinically approved photosensitizer, Photofrin®, and the pro-drug 5-aminolevulinic acid (PI: >7 relative to PI: >1 and PI: 4.4 for 5-aminolevulinic acid and Photofrin®, respectively). Furthermore, the ruthenium complexes were noted to show appreciable long-term cytotoxicity upon light irradiation in HeLa cells in a concentration-dependent manner. Consequently, this long-term activity of the ruthenium(II) polypyridyl complexes embodies their ability to reduce the probability of the recurrence of cervical cancer. Taken together, this presents a strong motivation for the development of polymetallic complexes as anticancer agents.

1. Introduction

The development of new chemotherapeutic treatments to circumvent drug resistance for long-term use, has become one of the important research thrusts in the battle against cancer. Since the discovery of cisplatin, several platinum-based metallodrugs have been developed, including the clinically used carboplatin and oxaliplatin [1,2]. However, the use of these metallodrugs is hindered by the same hurdles that limit the application of cisplatin, including off-target effects, the development of tumour drug resistance and a limited range of activity [3,4]. These limitations have resulted in a redirection in metallodrug discovery to other platinum-group metals, with ruthenium-based complexes representing the vanguard of research into the development of metallodrugs based on alternative platinum-group metals. This is exemplified by several ruthenium-based complexes including NAMI-A, NKP-1339 and TLD1433 having been clinically investigated for the treatment of various cancers [5–7].

In recent years, photodynamic therapy (PDT) has evolved as a successful alternative or adjuvant treatment modality for cancer. This is due to the non-invasive characteristics of PDT agents which provide spatial and temporal control over cell death [8–12]. PDT is a form of local light-based therapy in which Reactive Oxygen Species (ROS), generated photochemically by nontoxic photosensitizers (PS), induce oxidative damage to the essential cell and tissue components, bringing about cell and tissue death [13–15]. PDT is a two-step procedure, consisting of the administration of the PS, followed by exposure to light. This two-step procedure significantly reduces side effects, as the nontoxic PS is solely activated by light [16].

Ruthenium(II) polypyridyl complexes have remained amongst the most studied transition metal complexes in light-driven applications, including PDT, photocatalysis and luminescent sensing [7,17–20]. The interest in ruthenium(II) complexes stems from their favourable and conferrable characteristics, which can be fine-tuned to yield excited states that are accessible to visible light [21,22]. Indeed, ruthenium(II) polypyridyl complexes have garnered a considerable amount of interest in their development as photoactive agents, in the treatment of cancer, and continue to yield prolific results [21,23–27].

Combining photosensitizers with suitable pharmacophoric ligands is

* Corresponding author.
E-mail address: gregory.smith@uct.ac.za (G.S. Smith).

https://doi.org/10.1016/j.jinorgbio.2024.112545
Received 6 December 2023; Received in revised form 23 March 2024; Accepted 24 March 2024
Available online 26 March 2024

of paramount importance to metallodrug design in an effort to improve the photophysical properties of photosensitizers. The broad biological properties conferred by the benzimidazole scaffold and the benefit of incorporating this scaffold onto organometallic complexes is now well documented in the literature [28–31]. However, reports on the use of the benzimidazole scaffold as an ancillary ligand in the design of PSs for PDT are sparse [32–34].

The advantages of the incorporation of more than one metal center as part of a potential photosensitizer are well documented in the literature, as ruthenium(II)-based homo- and hetero-polynuclear complexes generally show enhanced phototoxicity relative to their mononuclear counterparts [35–40]. Furthermore, a similar trend can be observed when comparing the antiproliferative activity of cisplatin to that of its trinuclear conjugate, BBR3464, where the activity of trinuclear complex is superior relative to the analogous mononuclear counterpart [41,42]. Despite this, the development of polymetallic metallodrugs and metal-organic PSs for PDT remains in its infancy and relatively unexplored.

Herein, we report the synthesis of a series of trinuclear 2-pyridyl- and 2-quinolylbenzimidazole-based ruthenium(II) complexes and discuss their phototoxic activity as PDT agents in the HeLa cervical cancer cell line.

2. Results and discussion

2.1. Synthesis and characterization of the ruthenium complexes

The synthesis of the key *s*-triazine-anchored 2-pyridylbenzimidazole ligand (**6**) was carried out *via* a six-step procedure (Scheme 1) involving the i) *tert*-butyloxycarbonyl (Boc) protection of 1,3-diaminopropane, yielding **1**; ii) nucleophilic aromatic substitution reaction of **1** with 1-fluoro-2-nitrobenzene, to yield the aryl nitro precursor (**2**); iii) reduction of the aryl nitro precursor (**2**), with zinc in the presence of ammonium chloride, to produce the aryl 1,2-diamine (**3**); iv) the cyclocondensation of **3** with 2-pyridinecarboxaldehyde in the presence of a catalytic amount of trifluoracetic acid (TFA), yielding the 2-pyridylbenzimidazole (**4**); v) Boc-deprotection of **4** using an excess of TFA to yield **5**; vi) reaction of **5** with cyanuric chloride in *N,N*-dimethylformamide to yield the *s*-triazine anchored 2-pyridylbenzimidazole ligand (**6**).

In support of this study, the analogous trimeric and monomeric 2-pyridylbenzimidazole (**9** and **13**) and 2-quinolylbenzimidazole (**10**) ligands (based on a trisamine core) were synthesized in parallel, as described in the literature (Fig. 1) [28,41,43].

The synthesis of the polymetallic ruthenium(II) polypyridyl complexes (**Ru-1**, **Ru-2**, **Ru-3**) and mononuclear complex (**Mono**) was achieved in two steps: i) firstly, by the reaction of the appropriate benzimidazole-based ligand with dichloridobis(bipyridine)ruthenium (II) in ethanol at 78 °C overnight; ii) secondly, a salt metathesis reaction using ammonium hexafluorophosphate to yield the desired complexes as hexafluorophosphate salts (Fig. 2). The ruthenium(II) complexes were characterized by nuclear magnetic resonance (NMR) spectroscopy (Fig. S5-S7 in the ESI), high-resolution electrospray ionization mass spectrometry (HR-ESI) and purity confirmed by liquid chromatography.

2.2. Photophysicochemical properties

The emission and singlet oxygen quantum yields (ϕ_{em} and ϕ_{Δ} respectively) of the ruthenium(II) compounds were determined using reported comparative methods [44,45]. Tris(bipyridine)ruthenium(II) chloride ($[Ru(bpy)_3Cl_2]$) served as a benchmark with ϕ_{Δ} and ϕ_{em} values of 0.57 and 0.018 obtained in aerated DMF and acetonitrile, respectively [46–48].

2.2.1. Emission spectra and Emission Quantum Yield (ϕ_{em})

All the experiments were conducted in acetonitrile and the absorbance of the complexes at the excitation wavelength was maintained at 0.05 a.u. The 2-pyridylbenzimidazole-based complexes (**Ru-1**, **Ru-2** and **Mono**) were noted to show emission maxima in the range 650–665 nm, however, the emission maximum of the 2-quinolylbenzimidazole-based complex (**Ru-3**) was noted to be significantly red-shifted (759 nm). This is attributed to the extended aromatic ring inherent in complex **Ru-3**, which results in an emission maximum at a longer wavelength. The calculated emission quantum yields for the complexes are as follows: 8.6%, 2.6%, 5.1% and 0.95% for **Mono**, **Ru-1**, **Ru-2** and **Ru-3**, respectively (Table 1). The significantly lower emission quantum yields for the trinuclear complexes (**Ru-1**, **Ru-2**, **Ru-3**) may be ascribed to non-radiative dissipation of the excited state of these trinuclear complexes, and transient electron transfer between the excited ruthenium trisbipyridyl metal centers and either the triazine or trisalkylamine cores of the respective trinuclear complexes [49–53].

2.2.2. Singlet oxygen quantum yield (ϕ_{Δ})

Singlet oxygen is formed *via* an energy transfer process between the triplet excited state and molecular oxygen, widely referred to as the Type II reaction [54]. The ϕ_{Δ} values were determined using an indirect method, in which the photobleaching of 9,10-dimethylanthracene (DMA) was monitored in DMF after irradiation with blue light at 455 nm (330 mW.cm^{-2}). Solutions of the ruthenium(II) complexes, the $[Ru(bpy)_3Cl_2]$ standard (at 15 μM, respectively) and DMA (at 25 μM) were prepared in DMF. The photodegradation of DMA was evidenced by the decrease in absorbance at 402 nm, as illustrated in Fig. 3, in which DMA is degraded in the presence of the mononuclear complex (**Mono**) (Fig. 3a) and the trinuclear complex (**Ru-1**) (Fig. 3b).

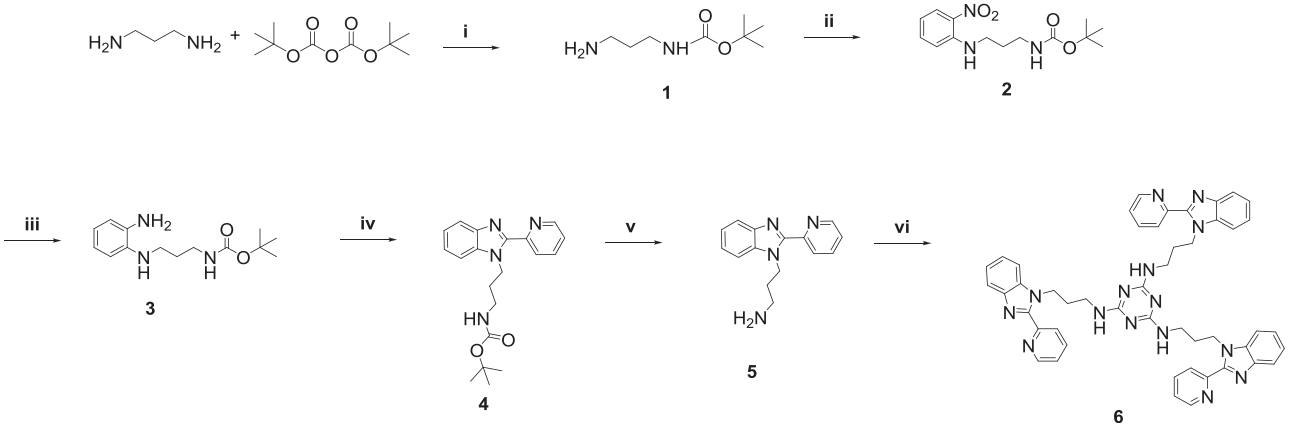

Scheme 1. Reagents and conditions: i) Diaminopropane/ $Boc_2(O)$/ $CHCl_3$/ RT/ 3 h; ii) 1-Fluoro-2-nitrobenzene/ DMF/ 100 °C/ 24 h; iii) Zn/ NH_4Cl/ MeOH/ RT/ 1 h; iv) 2-pyridinecarboxaldehyde/ TFA/ EtOH/ $MgSO_4$/ RT/ 24 h; v) TFA/ DCM/ 30 °C/ 24 h; vi) DMF/ K_2CO_3 /120 °C/ 48 h.

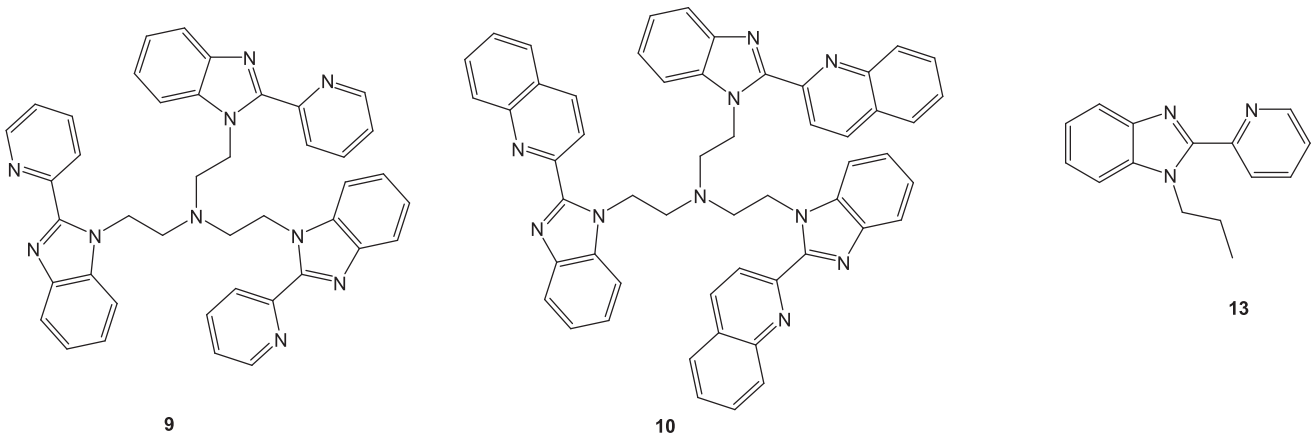

Fig. 1. The structures of the trisamine anchored trimeric 2-pyridyl (**9**) and 2-quinolylbenzimidazole-based (**10**) ligands and the corresponding monomeric 2-pyridylbenzimidazole congener (**13**).

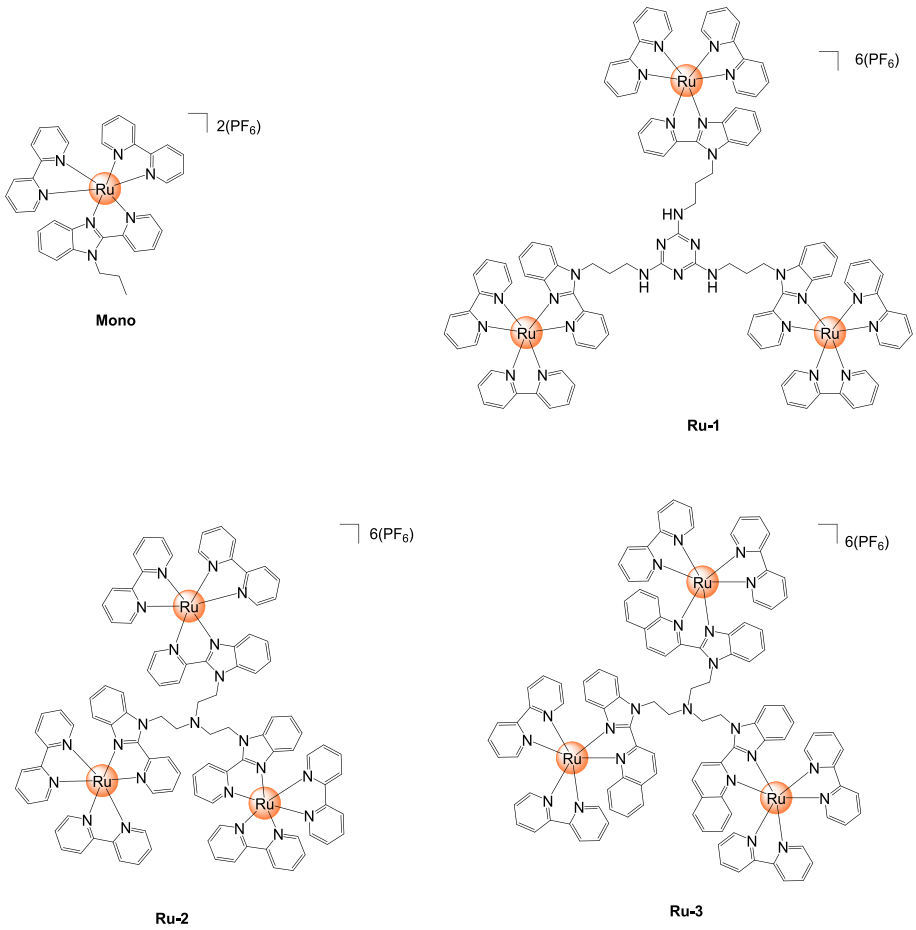

Fig. 2. The structures of the mononuclear 2-pyridylbenzimidazole-based ruthenium(II) polypyridyl complex (**Mono**) and the corresponding triazine-anchored (**Ru-1**) and trisamine anchored trinuclear complexes (**Ru-2** and **Ru-3**).

Table 1
Photophysical parameters of the ruthenium(II) polypyridyl complexes.

Compound	λ^{a}_{ex}	λ^{a}_{em}	φ^{a}_{Δ}	Φ^{b}_{em}
Mono	469	664	0.79	0.09
Ru-1	472	674	0.26	0.03
Ru-2	465	653	0.31	0.05
Ru-3	503	759	0.13	0.01

a: Parameter determined in acetonitrile; ***b***: parameter determined in DMF.

As previously observed for the emission quantum yields, the trinuclear complexes (**Ru-1**, **Ru-2**,

Ru-3) have significantly less singlet oxygen quantum yields relative to the mononuclear complex (**Mono**). This may in part be attributed to the increased flexibility of the trinuclear complexes, thus increasing the probability of non-radiative dissipation of the excited state *via* vibrational relaxation and/or kinetic energy [49–51]. The trend in the calculated ϕ_{Δ} values is, as for the emission quantum yields, of the following order: **Mono** > **Ru-2** > **Ru-1** > **Ru-3** (Table 1).

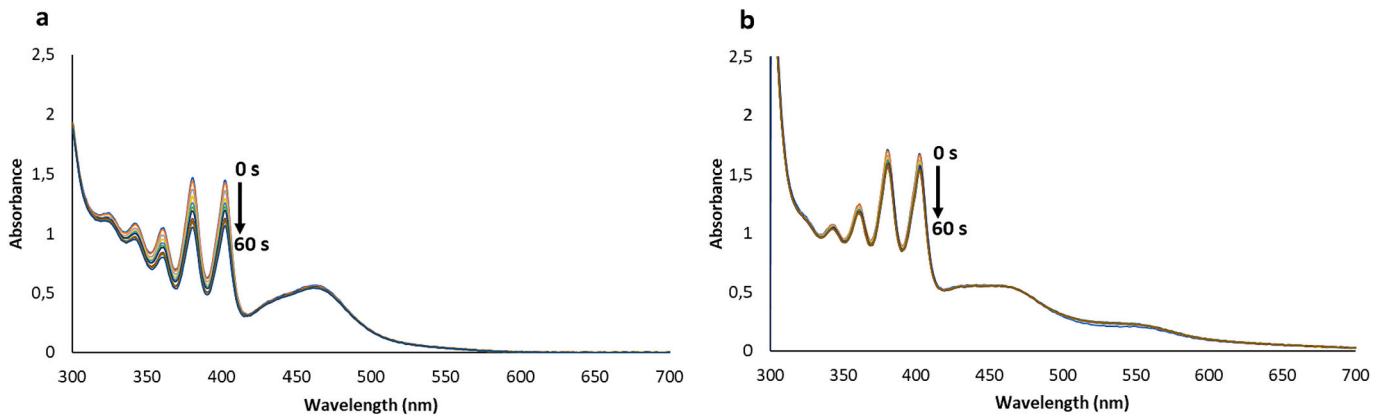

Fig. 3. The degradation of 9,10-dimethylanthracene (DMA) in the presence of either **Mono** (a) or **Ru-1** (b) in DMF over 60 s.

With this in mind, the ability of the ruthenium(II) complexes to generate $^1O_2$ in aqueous media (~1% DMSO in deionized H_2O) was investigated using 9,10-anthracenediyl-bis(methylene)dimalonic acid (ADMA) as a singlet oxygen quencher. All the complexes were noted to produce singlet oxygen species (Fig. S20), indicated by the time-dependent reduction of the absorbance of ADMA at 400 nm (Fig. 4, in which ADMA is being degraded in the presence of complex **Ru-2**).

However, the singlet oxygen quantum yields of the ruthenium(II) polypyridyl complexes were not calculated in aqueous media. This is due to the interaction of the endoperoxide (formed upon the irreversible reaction of ADMA with singlet oxygen) with the respective complexes, resulting in precipitation of the complexes out of solution (see Fig. S21a). Despite this, all the complexes have demonstrated the ability to generate singlet oxygen in aqueous media and dichlorodihydrofluorescein diacetate (DCFDA) assays confirm the ability of the complexes to produce ROS *in vitro* upon irradiation (Fig. S25).

2.3. Phototoxicity studies

To evaluate the potential of the trinuclear ruthenium complexes as PDT agents, their toxicity in the dark as well as upon light irradiation in the human cervical cancer cell line (HeLa) was evaluated using the WST-1 assay. The dark toxicity of the complexes was performed at gradient concentrations of 5–300 μM. Of note, none of the compounds inhibited HeLa cell survival to ≤50% in the absence of light with IC_{50} > 300 μM (Fig. S22). These results bode extremely well for the potential application of these complexes as PSs for PDT and are comparable with that of Prajith and co-workers who reported two trinuclear complexes of a similar structural motif with IC_{50} values of 287 μM and 280 μM [55]. Upon irradiation of the compounds with a blue LED light at 455 nm (330 mW.cm^{-2}), a general concentration-dependent reduction in HeLa cell survival was noted (Fig. S22), and the IC_{50} values of the complexes are summarized in Table 2. Generally, there was no discernible correlation between the singlet oxygen quantum yields of the trinuclear complexes and their phototoxicity. This is particularly self-evident for complex **Ru-3**, which has the lowest singlet oxygen quantum yield (ϕ_Δ = 0.13) but was one of the most active complexes (IC_{50} = 34.63 μM). This may be attributed to the fact that ruthenium complexes have been reported to indiscriminately exploit both type I and type II PDT mechanisms, and this may lead to the observation of no correlation between the singlet oxygen quantum yields and the observed phototoxicity [56–58].

The phototoxicity of the complexes follows the general trend: **Ru-2** ≈ **Ru-3** > **Ru-1** > **Mono**. Structurally, complex **Ru-1** consists of the

Table 2
The *in vitro* cytotoxicity (dark) and phototoxicity of the ruthenium(II) polypyridyl complexes on human cervical cancer cells (HeLa).

Compound	Light IC_{50} (μM)[b]	Dark IC_{50} (μM)	P.I.[a]
Mono	>45	>300	N/A
Ru-1	42.53 ± 1.16	>300	>7.05
Ru-2	34.05 ± 1.09	>300	>8.81
Ru-3	34.63 ± 1.11	>300	>8.66
Cisplatin [59]	–	7.6	–

a: Phototoxicity Index: IC_{50} Dark/ IC_{50} Light; *b*: 24 h incubation in HeLa cells in the dark followed by exposure to a 455 nm Thorlabs M455L3 blue LED (330 mW.cm^{-2} or 1188 J/cm^2) for 60 min.

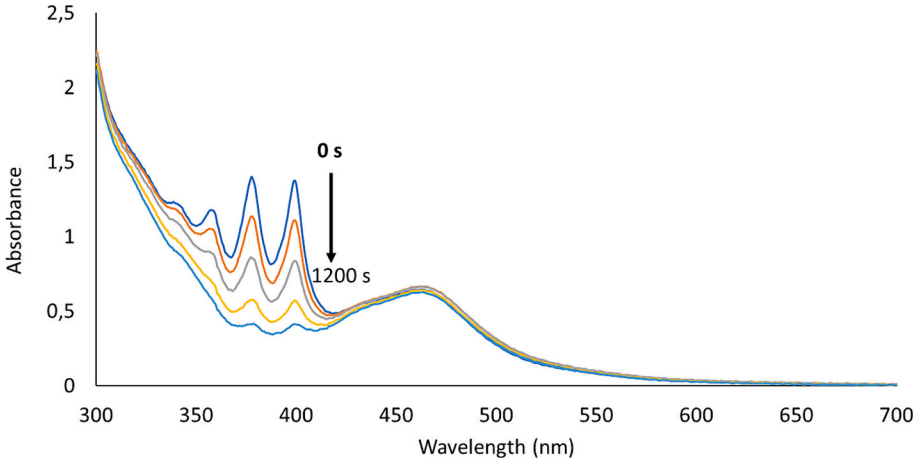

Fig. 4. The degradation of 9,10-anthracenediyl-bis(methylene)dimalonic acid (ADMA) in the presence of **Ru-2** in aqueous media over 1200 s.

pharmacologically privileged *s*-triazine core, which is contained in several FDA-approved drugs [60]. Additionally, *s*-triazine derivatives have been noted to have several protein targets, ranging from cyclin-dependent kinase (CDK) to dihydrofolate reductase, depending on the chemical structure [61]. However, the data generated shows that changing the trisamine core (in complexes **Ru-2** and **Ru-3**) to the *s*-triazine core (in complex **Ru-1**) does not significantly improve the phototoxicity, as we had initially envisaged, as the *s*-triazine-based complex (**Ru-1**) is the least active trinuclear complex ($IC_{50} = 42.53$ μM).

To explore the effect of the 2-aryl functionality of the benzimidazole scaffold, the trinuclear trisamine anchored 2-pyridyl (**Ru-2**) and 2-quinolinyl (**Ru-3**) benzimidazole-based complexes were evaluated for their phototoxicity. The positive effects that an extended pi-system exerts on the photophysical properties and the phototoxicity of ruthenium complexes are well documented in the literature [62–64]. From the data generated, there was no statistically significant difference in the phototoxicity of complexes **Ru-2** and **Ru-3** in the HeLa cell line (with comparable IC_{50} values of 34.05 ± 1.09 μM and 34.63 ± 1.11 μM, respectively). This observation was counter-intuitive, as with previous studies the extension of the pi-system on the 2-position of the benzimidazole scaffold resulted in the enhancement of the antiproliferative activity of structurally similar ruthenium(II)-*p*-cymene complexes [43].

A comparison of the phototoxicity of the mononuclear complex (**Mono**) to that of the trinuclear complexes reveals that the trinuclear complexes generally show enhanced phototoxicity in the tested cell line. This may be attributed in part to two factors: increased nuclearity and overall charge density. Prajith and *co*-workers recently reported a direct proportionality of the nuclearity of structurally similar ruthenium(II) polypyridyl complexes to the cellular uptake [55]. Additionally, Matshitse and co-workers reported the direct correlation between the overall charge of metal complexes and their cellular uptake [65]. Thus, we attribute the low activity of the mononuclear complex (**Mono**) to its low nuclearity (one metal center *vs.* three) and relatively lower charge (dicationic *vs* hexacationic). As such, these factors merit opportunities for the further development and study of trinuclear, highly charged metallodrugs as potential PDT agents.

2.4. Clonogenic assays

The treatment of cervical cancer patients with advanced stage or recurrent tumours remains a major hurdle, and this is reflected in the very low five-year survival rates of <5%, despite intensive therapy [66–68]. Moreover, the development of drug resistance by recurrent cervical cancer highlights the need for the identification of potential therapeutic agents which exhibit long-term cytotoxicity [69]. To this end, we investigated the long-term cytotoxic activity of the ruthenium (II) polypyridyl complexes (**Ru-2** and **Ru-3**), which showed the most promising activity in the short-term viability assay (WST-1 assay), using clonogenic assays. Furthermore, the mononuclear congener (**Mono**) was included in these experiments to corroborate the benefit of having more than one ruthenium(II) metal center on the long-term cytotoxicity of the tested trinuclear complexes. The clonogenic assay entails treating cells with the selected complexes (**Mono**, **Ru-2** and **Ru-3**) at various concentrations (½ IC_{50}, IC_{50} and 2× IC_{50}) for 24 h. Thereafter, a set of cells were irradiated with a blue LED light at 455 nm (330 $mW.cm^{-2}$) for 60 min, and another set of cells was maintained in the dark. This was followed by the replating of the cells at lower densities in drug-free media and the cells were allowed to grow over 12–15 days (with drug free growth media being replenished every 2 to 3 days).

When the HeLa cells were treated and maintained in the absence of light (Fig. 5a and c), all the tested complexes showed a concentration-dependent reduction of their long-term survival. However, it is worth noting that the dark activity of the **Ru-2** and **Ru-3** trimetallic ruthenium (II) complexes surpassed that of the mononuclear congener (**Mono**).

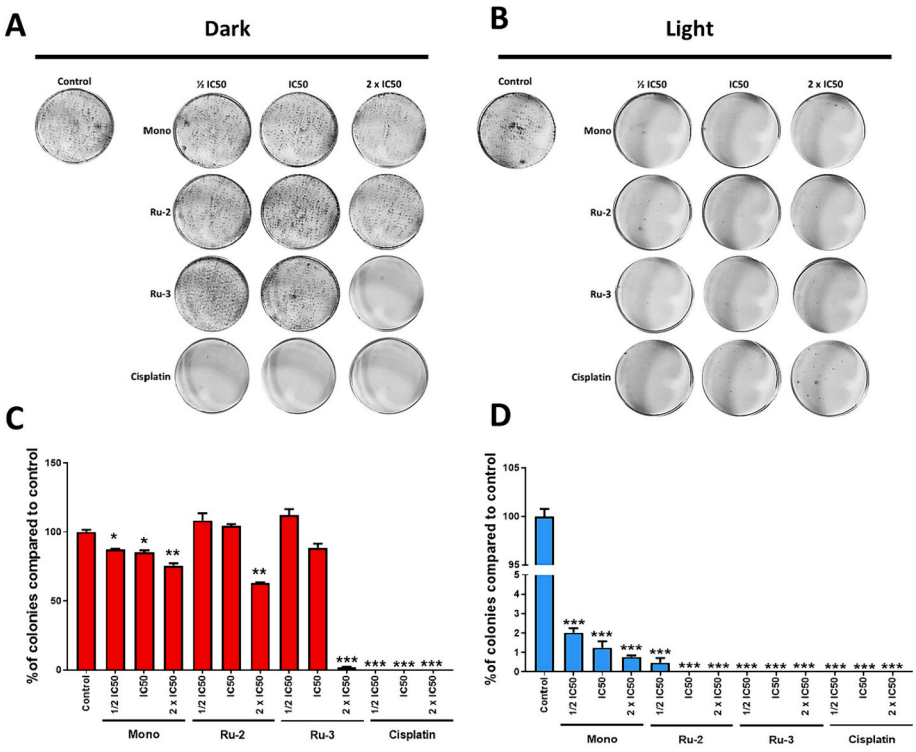

Fig. 5. Representative images and quantification of clonogenic assays of HeLa cells treated with ½ IC_{50}, IC_{50} and 2× IC_{50} concentrations of the trinuclear complexes (**Ru-2** and **Ru-3**) and the mononuclear complex (**Mono**) for 24 h, and either maintained in the dark (A and C) or irradiated with blue light (455 nm) for 60 min (B and D). Cells were replated at lower densities and maintained in drug-free media for 12–15 days and crystal violet-stained colonies were imaged and quantified using ImageJ. The graphs represent the mean colony area ± SEM for each treatment condition as a percentage of the vehicle control (untreated). Cisplatin was included as a positive control. (For interpretation of the references to colour in this figure legend, the reader is referred to the web version of this article.)

More noteworthy, complex **Ru-3** nearly eradicated HeLa colonies at the highest treated concentration (2× IC_{50}).

Relative to the HeLa cells that were maintained in the dark, upon light irradiation for 60 min (455 nm, 330 mW.cm^{-2}), a striking reduction in the colony forming ability of HeLa cells was observed when treated with all three tested compounds individually at all tested concentrations (Fig. 5b and d). Indeed, the images show that following light irradiation, there was an almost complete absence of colonies of HeLa cells treated with complexes **Ru-2** and **Ru-3** (Fig. 5b). These data are important as they further validate the phototoxic effects of the tested ruthenium(II) polypyridyl complexes against cervical cancer cells with the trinuclear complexes **Ru-2** and **Ru-3** being highly effective relative to the **Mono** complex, lending impetus to the use of polymetallic complexes.

3. Conclusions

A series of trinuclear hexacationic ruthenium(II) benzimidazole-based complexes (**Ru-1, Ru-2**, **Ru-3**) and a corresponding mononuclear congener (**Mono**) were synthesized and fully characterized. Investigation of the photophysical properties of the complexes revealed their ability to produce singlet oxygen upon irradiation in DMF (ϕ_Δ = 0.13–0.79) and aqueous media. When evaluated for their dark toxicity in the human cervical cancer cell line (HeLa), the compounds did not show a reduction in cell survival of 50% or below. Upon light irradiation, all the trinuclear complexes (**Ru-1**, **Ru-2** and **Ru-3**) show concentration-dependent antiproliferative activity, with IC_{50} values ranging between 34.05 μM and 42.53 μM. Despite the mild activity of the complexes, it is worth noting that all the complexes exhibit enhanced phototoxicity indices (PI in the range: 7.05–8.81) relative to those reported for clinically administered Photofrin® (PI: 4.4) [70] and 5-aminolevulinic acid (PI: >1) in the HeLa cell line [71]. Furthermore, the investigation of the long-term activity of selected complexes (**Mono**, **Ru-2** and **Ru-3**) revealed that all the tested complexes show mild dark cytotoxicity. However, upon light irradiation, the long-term cytotoxicity of complexes **Mono**, **Ru-2** and **Ru-3** is significantly enhanced, in a dose-dependent manner. The superior cytotoxicity of the trinuclear complexes (**Ru-2** and **Ru-3**) relative to the mononuclear congener (**Mono**) is evident once more, as complexes **Ru-2** and **Ru-3** show enhanced long-term phototoxicity in HeLa cells in comparison with the mononuclear complex (**Mono**).

Overall, the short- and long-term photocytotoxicity of the trinuclear complexes (**Ru-1, Ru-2, Ru-3**), surpasses that of the corresponding mononuclear complex (**Mono**). Although we are currently investigating strategies to enhance the generally modest biological activity of the complexes reported in this study, this study lends impetus to the development of polynuclear metallodrugs as potential PDT agents.

4. Experimental

4.1. General remarks

All reactions were carried out in an inert argon atmosphere unless stated otherwise. All reagents were purchased from commercial sources (Sigma-Aldrich, Combi-blocks) and used without further purification. Solvents were reduced at 40 °C in reduced pressure using a Büchi Rotavapor. The heat to reactions conducted above room temperature was supplied by a hot plate and silicone oil. All aqueous solutions were prepared using deionized water. Reactions were monitored by TLC using aluminium-backed Merck silica-gel F254 plates, and compounds were visualized under a UV lamp. All column chromatography was carried out using Fulka Silica Gel 60, 40–63 μm. Nuclear Magnetic Resonance spectra were recorded on either a Bruker X400 MHz spectrometer (^{1}H at 399.95 MHz and ^{13}C at 100.65 MHz) or a Varian Mercury XR300 MHz (^{1}H at 299.95 MHz, ^{13}C at 75.46 MHz) with tetramethylsilane (TMS) as the internal standard for chemical shifts. Chemical shifts and J-coupling values were reported in ppm and Hz, respectively. Infrared spectroscopy was conducted on a Perkin-Elmer Spectrum 100 FT-IR spectrometer using Attenuated Total Reflectance (ATR) with bond vibrations measured in reciprocal centimetres (cm^{-1}). Mass Spectrometry (MS) determinations were carried out using Electron Impact (EI) on JEOL GCmatell instrument or Electrospray Ionization (ESI) on a Waters API Quattro Micro triple quadrupole mass spectrometer with data recorded using the positive mode. A Büchi Melting Point Apparatus B-540 machine was used to obtain the uncorrected melting points of each compound. UV/ Vis electronic spectra were recorded on a Shimadzu UV-2550 spectrophotometer. Ambient temperature fluorescence spectra were measured on a Cary Eclipse Fluorescence Spectrophotometer (G9800A). The purity of the complexes was determined using an Agilent HPLC 1260 equipped with an Agilent DAD 1260 UV/ Vis detector and an Agilent Pursuit 5 C18 column (5 μM, 150 mm × 4.6 mm). The compounds were eluted using a mixture of solvent A (0.1% trifluoroacetic acid in deionized water) and solvent B (methanol) at a flow rate of 0.5 mL/ min. The gradient elution conditions were as follows: 90% solvent A between 0 and 2 min, 90–10% solvent A from 2 to 8 min, 10% solvent A from 8 to 20 min. The compounds, *cis*-dichlorobis(bipyridine)ruthenium (II), *tert*-butyl (3-aminopropyl)carbamate (**1**), 3-(2-(pyridin-2-yl)-1*H*-benzo[*d*]imidazol-1-yl)propan-1-amine (**5**), N^1-(2-nitrophenyl)-N^2,N^2-bis(2-((2-nitrophenyl)amino)ethyl)ethane-1,2-diamine (**7**), N^1-(2-(bis(2-((2-aminophenyl)amino)ethyl)amino)ethyl)benzene-1,2-diamine (**8**), tris(2-(2-(pyridin-2-yl)-1*H*-benzo[*d*]imidazol-1-yl)ethyl)amine (**9**) and tris(2-(2-(quinolin-2-yl)-1*H*-benzo[*d*]imidazol-1-yl)ethyl)amine (**10**) [43], 2-nitro-*N*-propylaniline (**11**), N^1-propylbenzene-1,2-diamine (**12**) and 1-propyl-2-(pyridin-2-yl)-1H-benzo[*d*]imidazole (**13**), were synthesized following published literature methods [28,41,72,73].

4.2. Synthesis of the 2-pyridylbenzimidazole s-triazine ligand (6)

4.2.1. Synthesis of tert-butyl (3-((2-nitrophenyl)amino)propyl)carbamate (2)

Tert-butyl (3-aminopropyl)carbamate (**1**) (1.25 g, 7.28 mmol) was added to DMF (10 mL) at room temperature. Thereafter, 1-fluoro-2-nitrobenzene (1.15 mL, 10.9 mmol) was added and the reaction mixture was allowed to stir at 100 °C for 24 h. Upon complete reaction of the starting material, the reaction mixture was diluted with toluene (250 mL) and the solvent was removed using rotary evaporation. The resultant crude residue was re-dissolved in 100 mL of dichloromethane (DCM) and washed with a saturated brine solution (80 mL) and extracted with two more aliquots of DCM (2 × 100 mL). The organic extracts were collected and dried over anhydrous sodium sulfate, and excess solvent was reduced *in vacuo*. The desired product (**2**) was isolated by column chromatography as a yellow powder (1.59 g, 5.45 mmol). **R_f (3:1 petroleum ether: ethyl acetate):** 0.50. **Yield:** 75%. **^{1}H NMR (300 MHz, $CDCl_3$) δ (ppm)**: 8.17 (ddd, J = 8.6, 4.2, 1.4 Hz, 1H, ArH), 8.06 (s, 1H, ArH), 7.50–7.37 (m, 1H, ArH), 6.85 (dd, J = 8.6, 5.3 Hz, 1H, ArH), 6.72–6.58 (m, 1H, ArH), 4.62 (s, 1H, NH), 3.50 (t, J = 6.3 Hz, 1H, CH_2), 3.37 (t, J = 7.0 Hz, 2H, CH_2), 3.32–3.20 (m, 2H, CH_2), 2.26–2.07 (m, 1H, CH_2), 2.00–1.82 (m, 2H, CH_2), 1.45 (s, 9H, CH_3). **^{13}C NMR (101 MHz, $CDCl_3$) δ (ppm)**: 156.09, 145.40, 136.28, 131.95, 126.95, 115.34, 113.67, 79.49, 40.50, 38.25, 29.62, 28.39. **EI-MS (*m/z*)**: Observed: 296.2 (25% $[M + H]^+$, Calculated: 296.2. **FT-IR** (ATR) ν (cm^{-1}): 1510 (N—O stretch). **MP** (°C): 89.7–91.2 °C.

4.2.2. Synthesis of tert-butyl (3-((2-aminophenyl)amino)propyl)carbamate (3)

Tert-butyl (3-((2-nitrophenyl)amino)propyl)carbamate (**2**) (1.59 g, 5.38 mmol) was dissolved in anhydrous methanol (10 mL) and allowed to stir for 5 min. Ammonium chloride (2.92 g, 54.5 mmol) and zinc powder (7.13 g, 107 mmol) were added, and the resultant mixture was allowed to stir at room temperature for 1 h. The reaction mixture was filtered through Celite® and rinsed with copious methanol. The filtrate was subsequently collected, and the excess solvent was reduced by

rotary evaporation. The resultant residue was redissolved in DCM (100 mL) and washed with two aliquots of a saturated brine solution (2 × 100 mL) and deionized water (100 mL). The organic extract was collected, dried over anhydrous sodium sulfate and excess solvent was reduced *in vacuo* and the resultant crude product was purified using column chromatography (100% ethyl acetate). The desired compound (**3**) was isolated as a dark brown oil (0.813 g, 3.07 mmol). **R_f (ethyl acetate):** 0.82. **Yield**: 57%. **^{1}H NMR (300 MHz, $CDCl_3$) δ (ppm)**: 6.87–6.74 (m, 1H, ArH), 6.76–6.57 (m, 3H, ArH), 4.71 (s, 1H, NH), 3.37–3.13 (m, 6H, H-g, CH_2), 1.93–1.74 (m, 2H, CH_2), 1.45 (s, J = 17.8 Hz, 9H, CH_3). **^{13}C NMR (151 MHz, $CDCl_3$) δ (ppm)**: 156.19, 137.15, 134.50, 120.52, 118.88, 116.55, 112.15, 79.24, 41.57, 38.35, 29.70, 28.40. **EI-MS (*m/z*)**: Observed: 266.2 (100% $[M + H]^+$, Calculated: 266.2. **FT-IR** (ATR) ν (cm^{-1}): 1691 cm^{-1} (C═O stretch), 3378 cm^{-1} (1° NH_2 stretch).

4.2.3. Synthesis of tert-butyl (3-(2-(pyridin-2-yl)-1H-benzo[d]imidazol-1-yl)propyl)carbamate (4)

Tert-butyl (3-((2-aminophenyl)amino)propyl)carbamate (**3**) (0.100 g, 0.383 mmol) was dissolved in anhydrous ethanol (10 mL) and allowed to stir under argon for 5 min. Thereafter, 2-pyridinecarboxaldehyde (0.0550 mL, 0.575 mmol), trifluoracetic acid (TFA) (0.00293 mL, 0.0383 mmol) and magnesium sulfate (0.276 g, 2.29 mmol) were sequentially added to the reaction vessel. The reaction mixture was allowed to stir at 45 °C overnight. The reaction mixture was subsequently filtered, and the filtrate collected. The excess solvent was removed by rotary evaporation, and the resultant crude mixture was redissolved in dichloromethane (30 mL) and washed with a saturated sodium bicarbonate solution (30 mL) and a saturated brine solution (30 mL). The organic extracts were collected and dried over anhydrous sodium sulfate, and the excess solvent was removed *in vacuo*. Silica gel column chromatography was used to isolate compound **4** as a dark yellow oil (0.0898 g, 0.255 mmol). **R_f (Ethyl Acetate: Petroleum Ether 2:1):** 0.40. **Yield**: 68%. **^{1}H NMR (300 MHz, $CDCl_3$) δ (ppm):** 8.69 (dd, J = 2.3, 1.5 Hz, 1H, ArH), 8.39 (d, J = 8.0 Hz, 1H, ArH), 7.87–7.69 (m, 2H, ArH), 7.45–7.35 (m, 1H, ArH), 7.35–7.21 (m, 3H, ArH), 5.87 (s, 1H, NH), 4.79 (t, J = 7.0 Hz, 2H, CH_2), 3.12 (dd, J = 11.8, 5.8 Hz, 2H, CH_2), 2.18–2.04 (m, 2H, CH_2), 1.40 (s, 9H, CH_3). **^{13}C NMR (151 MHz, $CDCl_3$) δ (ppm)**: 156.05, 149.54, 149.07, 148.51, 141.47, 137.27, 135.87, 125.64, 124.28, 123.94, 123.31, 119.90, 110.44, 78.97, 43.07, 37.17, 29.84, 28.45. **EI-MS (*m/z*)**: Observed: 353.2 (100% $[M + H]^+$, Calculated: 353.2. **FT-IR** (ATR) ν (cm^{-1}): 1678 cm^{-1} (C═O stretch), 1580 (pyridyl C═N).

4.2.4. Synthesis of the s-triazine ligand N^2,N^4,N^6-tris(3-(2-(pyridin-2-yl)-1H-benzo[d]imidazol-1-yl)propyl)-1,3,5-triazine-2,4,6-triamine (6)

To a stirring solution of 3-(2-(pyridin-2-yl)-1*H*-benzo[*d*]imidazol-1-yl)propan-1-amine (**5**) (0.501 g, 1.98 mmol) in DMF (10 mL), cyanuric chloride (0.0978 g, 0.528 mmol) and potassium carbonate (0.274 g, 1.982 mmol) were sequentially added. The reaction mixture was stirred at 120 °C for 72 h. The reaction vessel was allowed to cool to room temperature and toluene (300 mL) was added. Excess solvent was removed *in vacuo* and the residue was re-dissolved in DCM (20 mL) and washed with two aliquots of a saturated brine solution (2 × 20 mL). The organic extracts were collected and dried over sodium sulfate. The excess solvent was removed *via* rotary evaporation and the crude residue was purified using column chromatography. Compound **6** was isolated as an off-white solid (0.539 g, 0.648 mmol). **R_f (2: 1 petroleum ether: ethyl acetate):** 0.48. **Yield**: 33%. **^{1}H NMR (400 MHz, DMSO) δ(ppm)**: 8.74 (d, J = 4.4 Hz, 3H, ArH), 8.33 (d, J = 7.9 Hz, 3H, ArH), 8.01 (t, J = 7.8 Hz, 3H, ArH), 7.68 (ddd, J = 22.7, 15.5, 7.8 Hz, 7H, ArH), 7.52 (dd, J = 7.9, 4.6 Hz, 4H, ArH), 7.37–7.17 (m, 7H, ArH), 6.91 (br s, 2H, NH), 5.75 (s, 1H, NH), 4.82 (t, J = 7.2 Hz, 6H, CH_2), 2.97 (dd, J = 12.5, 7.3 Hz, 6H, CH_2), 1.98–1.85 (m, 6H, CH_2). **^{13}C NMR (151 MHz, $CDCl_3$) δ (ppm)**: 156.03, 151.17, 149.66, 142.57, 137.89, 136.84, 124.69,123.69, 122.81, 122.32, 121.94, 120.02, 112.51, 111.23, 43.32, 38.13, 30.65. **FT-IR** (ATR) ν (cm^{-1}): 1680 (triazine C═N, and benzimidazole imine C═N), 1586 (pyridyl C═N). **EI-MS (*m/z*)**: Observed: 358.3 (100%, $[C_{18}H_{15}N_9 + H]^+$), Calculated: 358.3. **MP** (°C): 100.2–102.8.

4.3. The general synthesis of the ruthenium(II) polypyridyl complexes (Mono, Ru-1, Ru-2, Ru-3)

The appropriate trimeric 2-pyridylbenzimidazole ligand (1 eq.) (either N^2,N^4,N^6-tris(3-(2-(pyridin-2-yl)-1*H*-benzo[*d*]imidazol-1-yl)propyl)-1,3,5-triazine-2,4,6-triamine, tris(2-(2-(pyridin-2-yl)-1*H*-benzo[*d*]imidazol-1-yl)ethyl)amine or tris(2-(2-(quinolin-2-yl)-1*H*-benzo[*d*]imidazol-1-yl)ethyl)amine) was dissolved in anhydrous ethanol (5 mL). To this stirring solution, *cis*-dichlorobis(bipyridine)ruthenium(II) (3 eq.) was added and the reaction mixture was refluxed at 78 °C overnight. After 24 h, the reaction mixture was cooled to room temperature and a solution of ammonium hexafluorophosphate (6 eq.) in anhydrous ethanol (2 mL) was added, and the reaction mixture was stirred for an additional 30 min at room temperature. The contents of the reaction flask were subsequently filtered through Celite®. The solvent was removed under reduced pressure, which resulted in a solid precipitate. The desired complexes were isolated by suction filtration and washed with cold ethanol (10 mL).

4.3.1. The synthesis of the triazine-based ruthenium(II) polypyridyl complex (Ru-1)

The *s*-triazine ligand N^2,N^4,N^6-tris(3-(2-(pyridin-2-yl)-1*H*-benzo[*d*]imidazol-1-yl)propyl)-1,3,5-triazine-2,4,6-triamine, compound (**6**) (0.0301 g, 0.0361 mmol), was reacted with *cis*-dichlorobis(bipyridine) ruthenium(II) (0.0557 g, 0.115 mmol) under reflux at 78 °C overnight. Thereafter, NH_4PF_6 (0.0353 g, 0.217 mmol) was added and this mixture was allowed to stir for 1 h. The desired complex (**Ru-1**) was isolated as a burgundy solid (0.06737 g, 0.0325 mmol) by suction filtration and washed with cold ethanol (10 mL). **Yield**: 90%. **^{1}H NMR (600 MHz, DMSO) δ (ppm)**: 8.84 (d, J = 7.0 Hz, ArH), 8.75 (d, J = 8.0 Hz, 3H, ArH), 8.64 (d, J = 8.1 Hz, 3H, ArH), 8.24 (t, J = 7.6 Hz, 4H, ArH), 8.22–8.11 (m, 10H, ArH), 8.08 (t, J = 7.7 Hz, 3H, ArH), 7.96 (d, J = 8.4 Hz, 4H, ArH), 7.91 (d, J = 5.0 Hz, 3H, ArH), 7.84 (d, J = 5.0 Hz, 3H, ArH), 7.77 (s, 8H, ArH), 7.72 (d, J = 5.1 Hz, 4H, ArH), 7.64–7.40 (m, 22H, ArH), 7.13–7.03 (m, 6H, ArH), 5.76–5.66 (m, 3H, NH), 4.99–4.86 (m, 6H, CH_2), 3.03 (dt, J = 18.4, 6.1 Hz, 6H, CH_2), 2.08 (bs, 6H, CH_2). **^{13}C NMR (151 MHz, DMSO) δ (ppm)**: 158.17, 157.95, 157.85, 157.66, 157.61, 157.09, 156.40, 156.18, 155.64, 153.53, 153.20, 152.47, 152.24, 151.91, 151.76, 150.72, 149.46, 148.74, 140.46, 139.07, 138.99, 138.48, 138.21, 138.14, 138.07, 137.90, 136.76, 128.39, 128.30, 128.23, 128.03, 127.78, 127.31, 127.28, 126.34, 125.96, 125.49, 125.13, 124.99, 124.85, 124.77, 124.72, 124.47, 124.20, 123.82, 115.43, 115.43, 113.35, 113.35, 78.31, 78.31, 43.79, 43.73, 37.61, 29.78, 28.69, 28.69. **FT-IR** (ATR) ν (cm^{-1}): 1450 ($C=N_{imine}$), 834 (P—F). **MP** (°C): 224.6 (decomp.). **MS (HR-ESI, *m/z*)**: Observed: 325.0881 (60% $[C_{35}H_{30}N_7Ru]^{2+}$), Calculated: 325.0798. Purity: 98.45%, by LC (t_R = 2.034 min).

4.3.2. The synthesis of the trisamine-2-pyridylbenzimidazole ruthenium(II) polypyridyl complex (Ru-2)

The trisamine-based ligand, tris(2-(2-(pyridin-2-yl)-1*H*-benzo[*d*]imidazol-1-yl)ethyl)amine (**9**) (0.0447 g, 0.0588 mmol) was reacted with *cis*-dichlorobis(bipyridine)ruthenium(II) (0.0854 g, 0.1764 mmol) under reflux at 78 °C overnight. Thereafter, NH_4PF_6 (0.173 g, 1.06 mmol) was added and was allowed to stir for a further 1 h. The desired complex (**Ru-2**) was isolated as a dark red solid (0.0688 g, 0.0241 mmol) by suction filtration and washed with cold ethanol (10 mL). **Yield**: 42%. **^{1}H NMR (600 MHz, DMSO) δ (ppm):** 8.82–8.71 (m, 12H, ArH), 8.57 (t, J = 9.0 Hz, 3H, ArH), 8.48 (d, J = 9.3 Hz, 3H, ArH), 8.24–8.17 (m, 6H, ArH), 8.17–7.93 (m, 16H, ArH), 7.88–7.81 (m, 7H, ArH), 7.77 (t, J = 5.7 Hz, 3H, ArH), 7.72–7.44 (m, 34H, ArH), 7.29–6.97 (m, 22H, ArH), 5.77 (dd, J = 12.5, 8.4 Hz, 3H, ArH), 5.11–4.87 (m, 6H, CH_2), 3.50–3.34 (m,

7H, CH_2). **^{13}C NMR (151 MHz, DMSO) δ (ppm)**: 157.76, 157.64, 157.33, 156.96, 156.78, 156.67, 153.14, 152.05, 151.91, 151.50, 151.45, 151.34, 150.68, 150.53, 149.17, 148.43, 148.38, 140.54, 138.59, 138.51, 138.37, 138.28, 138.16, 138.11, 138.01, 137.13, 137.08, 128.31, 127.96, 127.52, 127.45, 126.42, 126.36, 125.77, 124.84, 124.74, 124.60, 124.05, 123.86, 115.79, 113.25, 112.98, 109.20, 53.55, 8.99. **FT-IR** (ATR) ν (cm^{-1}): 1438 ($C{=}N_{imine}$), 832 (P—F). **MP** (°C): 229.1 (decomp.). **MS (HR-ESI, *m/z*)**: Observed: 325.0867 (20% $[C_{34}H_{28}N_8Ru]^{2+}$), Calculated: 325.0735. Purity: 99.50%, by LC (t_R = 3.724 min).

4.3.3. The synthesis of the trisamine-2-quinolylbenzimidazole ruthenium (II) polypyridyl complex (*Ru-3*)

A mixture of the trimeric 2-quinolylbenzimidazole ligand, tris(2-(2-(quinolin-2-yl)-1*H*-benzo[*d*]imidazol-1-yl)ethyl)amine (**10**) (0.0520 g, 0.0602 mmol) and *cis*-dichlorobis(bipyridine)ruthenium(II) (0.0875 g, 0.181 mmol) was refluxed at 78 °C overnight. Thereafter, NH_4PF_6 (0.0588 g, 0.361 mmol) was added and allowed to stir for 1 h. The desired complex (**Ru-3**) was isolated as a red solid (0.142 g, 0.487 mmol) by suction filtration and washed with cold ethanol (10 mL). **Yield**: 80%. **^{1}H NMR (600 MHz, DMSO) δ (ppm)**: 8.91–8.78 (m, 2H, ArH), 8.74–8.69 (m, 1H, ArH), 8.59–8.43 (m, 8H, ArH), 8.40–8.20 (m, 7H, ArH), 8.13–7.67 (m, 20H, ArH), 7.62–7.36 (m, 14H, ArH), 7.28–7.18 (m, 8H, ArH), 7.17–6.97 (m, 8H, ArH), 6.87 (d, J = 8.1 Hz, 2H, ArH), 6.82–6.61 (m, 2H, ArH), 5,53 (t, J = 8,2 Hz, 3H, ArH),5.33–4.02 (m, 6H, CH_2), 3.13–2.93 (m, 6H, CH_2). **^{13}C NMR (151 MHz, DMSO) δ (ppm)**: 158.27, 157.42, 157.07, 156.99, 151.16, 150.13, 149.24, 146.61, 142.51, 141.08, 139.47, 139.07, 137.45, 137.24, 136.78, 132.05, 130.14, 129.87, 128.59, 128.42, 127.71, 127.61, 125.89, 125.03, 124.73, 124.04, 123.11, 121.73, 120.42, 115.73, 114.01, 110.53, 55.33, 54.41, 43.66, 40.88. **FT-IR** (ATR) ν (cm^{-1}): 1458 ($C{=}N_{imine}$), 836 (P—F). **MP** (°C): 234.7 (decomp.). **MS (HR-ESI, *m/z*)**: Observed: 415.1322 (100% $[C_{114}H_{91}N_{22}Ru_3]^{5+}$), Calculated: 415.0991. Purity: 98%, by LC (t_R = 2.009 min).

4.3.4. The synthesis of the ruthenium(II) polypyridyl complex (*Mono*)

The 1-propyl-2-(pyridin-2-yl)-1*H*-benzo[*d*]imidazole ligand (**13**) (0.0289 g, 0.122 mmol) was dissolved in anhydrous ethanol (5 mL) under argon. To this stirring solution, *cis*-dichlorobis(bipyridine)ruthenium(II) (0.0651 g, 0.134 mmol) was added and the reaction mixture was refluxed at 78 °C overnight. After 24 h, the reaction mixture was cooled to room temperature and a solution of ammonium hexafluorophosphate (0.0397 g, 0.244 mmol) in anhydrous ethanol (2 mL) was added, and the reaction mixture was stirred for an additional 30 min at room temperature. The contents of the reaction flask were subsequently filtered through Celite®. Excess DCM was removed under reduced pressure, which resulted in a burgundy solid precipitate. The desired complexes were isolated by suction filtration and washed with cold ethanol (10 mL). **Yield**: 97.1% **^{1}H NMR (600 MHz, DMSO) δ (ppm):** 8.84 (dd, J = 12.7, 5.7 Hz, 3H, ArH), 8.73 (d, J = 8.1 Hz, 1H, ArH), 8.64 (d, J = 8.3 Hz, 1H, ArH), 8.23 (dd, J = 14.9, 7.3 Hz, 2H, ArH), 8.16 (dt, J = 15.9, 7.9 Hz, 2H, ArH), 8.07 (t, J = 7.9 Hz, 1H, ArH), 8.00 (d, J = 8.5 Hz, 1H, ArH), 7.92 (d, J = 5.5 Hz, 1H, ArH), 7.92 (d, J = 5.5 Hz, 1H, ArH), 7.78 (ddd, J = 17.9, 15.9, 5.5 Hz, 4H, ArH), 7.59 (t, J = 6.6 Hz, 1H, ArH), 7.57–7.51 (m, 2H, ArH), 7.51–7.43 (m, 3H, ArH), 7.08 (t, J = 7.8 Hz, 1H, ArH), 5.71 (d, J = 8.3 Hz, 1H, ArH), 4.98–4.80 (m, 2H, CH_2), 2.00–1.85 (m, 2H, CH_2), 0.89 (t, J = 7.4 Hz, 3H, CH_3). **^{13}C NMR (151 MHz, DMSO) δ (ppm)**: 157.96, 157.61, 157.08, 153.09, 152.26, 151.83, 150.73, 148.78, 140.38, 138.69, 138.47, 138.20, 138.10, 137.93, 137.00, 128.37, 128.28, 128.21, 128.01, 126.32, 126.03, 125.4, 124.99, 124.87, 124.70, 124.43, 115.36, 113.60, 46.99, 23.02, 11.06. **FT-IR** (ATR) ν (cm^{-1}): 1446 ($C{=}N_{imine}$), 830 (P—F). **MP** (°C): 297.8 (decomp.). **MS (HR-ESI, *m/z*)**: Observed: 325.5878 (100% $[M\text{-}2PF_6]^{2+}$), Calculated: 325.5843. Purity: 97%, by LC (t_R = 2.799 min).

4.4. Photophysical and photochemical properties

Singlet oxygen quantum yields (ϕ_Δ) and emission quantum yields (ϕ_{em}) were determined using the comparative method, reported in the literature [44,45] with the necessary equations provided in the Supplementary Information. Tris(bipyridine)ruthenium(II) chloride ($[Ru(bpy)_3Cl_2]$) served as a benchmark with, ϕ_Δ and ϕ_{em} values of 0.57 and 0.018 in DMF and acetonitrile, respectively [46–48]. When calculating the singlet oxygen quantum yields (ϕ_Δ) the absorbance of the sample was not corrected for.

4.5. Cell culture

The HeLa cervical cancer cell line was cultured and maintained in Roswell Park Memorial Institute (RPMI) 1640 medium (Sigma Aldrich, USA). The growth medium was supplemented with 10% heat-inactivated foetal bovine serum, 100 μg/mL streptomycin, and 100 U/mL penicillin (Gibco, Life Technologies, USA). The cells were maintained in an environment with 5% CO_2 at 37 °C to maintain physiological pH and temperature respectively. The culture medium was replaced every 48–72 h.

4.5.1. Cytotoxicity studies

Briefly, HeLa cells were seeded at a density of 4500 cells/ well and consequently incubated at 37 °C for 48 h to enable adhesion. Thereafter, the cells were incubated for 48 h with either the vehicle control (0.1% DMSO) or various concentrations (5–35 μM) of the tested ruthenium(II) complexes. The original medium was removed after 48 h and replaced with fresh RPMI 1640 without phenol red. The cells were photo-irradiated with a 455 nm Thorlabs M455L3 LED for 60 min (330 mW.cm^{-2}). Fresh RPMI was subsequently added, and the cells were incubated for an additional 24 h. A separate set of cells were incubated with the tested complexes at concentrations ranging from 5 to 300 μM in the absence of light. Cell proliferation and viability were quantified by treating the cells with 4-(3-(4-iodophenyl)-2-(4-nitrophenyl)-2*H*-tetrazol-3-ium-5-yl)benzene-1,3-disulfonate (WST-1) according to a procedure described by Ishiyama et al. [74] The absorbance at 420 nm was measured with a Molecular Devices Spectra Max M5 plate reader. The absorbances recorded were appropriately adjusted for the growth media (RPMI 1640) and the respective complexes.

4.5.2. Intracellular ROS (DCFDA Assay)

The 2′,7′-dichlorodihydrofluorescein diacetate (DCFDA) assay was used to quantify the production of intracellular reactive oxygen species (ROS) by the ruthenium(II) complexes [75]. HeLa cells were plated at a density of 2 × 10^4 cells/ well and allowed to adhere overnight. After adhesion, the cells were incubated with 35 μM of each of the ruthenium (II) complexes for 4 h in the dark. Thereafter, DCFDA (at a concentration of 10 μM) was added and the cells were incubated in the dark for 30 min. The DCFDA solution was removed and the cells were washed three times with PBS to remove any extracellular DCFDA and ruthenium(II) complexes. The cells were subjected to irradiation with a ThorLabs 455 L3 LED for 15 min. Similarly, another 96-well plate was maintained in the dark. Fluorescence was measured using a multi-plate reader with excitation and emission wavelengths of 485 nm and 353 nm, respectively. H_2O_2 was used as a positive control and vehicle-treated (0.1% DMSO) cells were used as a negative control.

4.5.3. Clonogenic assays

HeLa cells were seeded at a density of 1.5 × 10^5 in 35 mm dishes and were incubated for 24 h at 37 °C to allow adhesion. Thereafter, the cells were treated with various concentrations ($^1/_2$ IC_{50}, IC_{50} and 2× IC_{50}) of selected ruthenium(II) polypyridyl complexes (**Ru-2**, **Ru-3** and **Mono**) or 0.1% DMSO (vehicle) for 24 h and were either maintained in the absence of light or photoirradiated with a 455 nm Thorlabs M455L3 LED for 60 min (330 mW.cm^{-2}). The cells were then subjected to clonogenic

assays in drug free media and surviving cells were determined after 12–15 days, as previously described by Kimani and co-workers [76].

CRediT authorship contribution statement

Athi Welsh: Writing – original draft, Investigation, Formal analysis, Data curation. **Refilwe Matshitse:** Writing – review & editing, Investigation, Data curation. **Saif F. Khan:** Writing – review & editing, Investigation, Data curation. **Tebello Nyokong:** Writing – review & editing, Resources. **Sharon Prince:** Writing – review & editing, Supervision, Resources, Project administration, Funding acquisition. **Gregory S. Smith:** Writing – review & editing, Supervision, Resources, Project administration, Funding acquisition, Conceptualization.

Declaration of competing interest

The authors declare that they have no known competing financial interests or personal relationships that could have appeared to influence the work reported in this paper.

Data availability

Data will be made available on request.

Acknowledgments

We gratefully acknowledge and thank the University of Cape Town, the National Research Foundation of South Africa (UID:129288, 120815), the International Centre for Genetic Engineering and Biotechnology (ICGEB), the DSI-CSIR Photonics Centre - African Laser Centre and the South African Medical Research Council (SAMRC) under a Self-Initiated Research Grant for financial support. The views and opinions expressed are those of the author(s) and do not necessarily represent the official views of the SAMRC.

Appendix A. Supplementary data

Supplementary data to this article can be found online at https://doi.org/10.1016/j.jinorgbio.2024.112545.

References

[1] Y.-P. Ho, S.C.F. Au-Yeung, K.K.W. To, Platinum-based anticancer agents: Innovative design strategies and biological perspectives, Med. Res. Rev. 23 (5) (2003) 633–655.
[2] C. Zhang, C. Xu, X. Gao, Q. Yao, Platinum-based drugs for cancer therapy and anti-tumor strategies, Theranostics 12 (5) (2022) 2115–2132.
[3] E.V. Sazonova, G.S. Kopeina, E.N. Imyanitov, B. Zhivotovsky, Platinum drugs and taxanes: can we overcome resistance? Cell Death Dis. 7 (1) (2021) 155.
[4] S. Jin, Y. Guo, Z. Guo, X. Wang, Monofunctional Platinum(II) Anticancer Agents, Pharmaceuticals 14 (2) (2021) 133–156.
[5] C.S. Allardyce, P.J. Dyson, Metal-based drugs that break the rules, Dalton Trans. 45 (2016) 3201–3209.
[6] G.K. Gransbury, P. Kappen, C.J. Glover, J.N. Hughes, A. Levina, P.A. Lay, I. F. Musgrave, H.H. Harris, Comparison of KP1019 and NAMI-A in tumour-mimetic environments, Metallomics 8 (2016) 762–773.
[7] J. Karges, Clinical Development of Metal Complexes as Photosensitizers for Photodynamic Therapy of Cancer, Angew. Chem. Int. Ed. 61 (5) (2022) e202112236.
[8] M.Á. Martínez, M.P. Carranza, A. Massaguer, L. Santos, J.A. Organero, C. Aliende, R. de Llorens, I. Ng-Choi, L. Feliu, M. Planas, A.M. Rodríguez, B.R. Manzano, G. Espino, F.A. Jalón, Synthesis and Biological Evaluation of Ru(II) and Pt(II) Complexes Bearing Carboxyl Groups as Potential Anticancer Targeted Drugs, Inorg. Chem. 56 (22) (2017) 13679–13696.
[9] K. Singha, P. Laha, F. Chandra, N. Dehury, A.L. Koner, S. Patra, Long-Lived Polypyridyl Based Mononuclear Ruthenium Complexes: Synthesis, Structure, and Azo Dye Decomposition, Inorg. Chem. 56 (11) (2017) 6489–6498.
[10] S.-Q. Zhang, T.-T. Meng, J. Li, F. Hong, J. Liu, Y. Wang, L.-H. Gao, H. Zhao, K.-Z. Wang, Near-IR/Visible-Emitting Thiophenyl-Based Ru(II) Complexes: Efficient Photodynamic Therapy, Cellular Uptake, and DNA Binding, Inorg. Chem. 58 (20) (2019) 14244–14259.
[11] J. Karges, H. Chao, G. Gasser, Critical discussion of the applications of metal complexes for 2-photon photodynamic therapy, J. Biol. Inorg. Chem. 25 (8) (2020) 1035–1050.
[12] S. Bonnet, Why develop photoactivated chemotherapy? Dalton Trans. 47 (31) (2018) 10330–10343.
[13] H. Kostron, T. Hasan, Photodynamic Medicine: From Bench to Clinic, Photodynamic Medicine: From Bench to Clinic, Royal Society of Chemistry, Cambridge, 2016.
[14] L.C.-C. Lee, K.K.-W. Lo, Luminescent and Photofunctional Transition Metal Complexes: From Molecular Design to Diagnostic and Therapeutic Applications, J. Am. Chem. Soc. 144 (32) (2022) 14420–14440.
[15] L. Zhang, N. Montesdeoca, J. Karges, H. Xiao, Immunogenic Cell Death Inducing Metal Complexes for Cancer Therapy, Angew. Chem. Int. Ed. 62 (21) (2023) e202300662.
[16] D.V. Straten, V. Mashayekhi, H.S.D. Bruijn, S. Oliveira, D.J. Robinson, Oncologic Photodynamic Therapy : Basic Principles , Current Clinical Status and Future Directions, Cancers (Basel) 9 (2) (2017) 19.
[17] S. Monro, K.L. Colon, H. Yin, J. Roque, P. Konda, S. Gujar, R.P. Thummel, L. Lilge, C.G. Cameron, S.A. McFarland, Transition Metal Complexes and Photodynamic Therapy from a Tumor-Centered Approach : Challenges , Opportunities , and Highlights from the Development of TLD1433, Chem. Rev. 119 (2019) 797–828.
[18] M.H. Keefe, K.D. Benkstein, J.T. Hupp, Luminescent sensor molecules based on coordinated metals: a review of recent developments, Coord. Chem. Rev. 205 (1) (2000) 201–228.
[19] C.K. Prier, D.A. Rankic, D.W.C. MacMillan, Visible Light Photoredox Catalysis with Transition Metal Complexes: Applications in Organic Synthesis, Chem. Rev. 113 (7) (2013) 5322–5363.
[20] J. Karges, T. Yempala, M. Tharaud, D. Gibson, G. Gasser, A Multi-action and Multi-target RuII–PtIV Conjugate Combining Cancer-Activated Chemotherapy and Photodynamic Therapy to Overcome Drug Resistant Cancers, Angew. Chem. Int. Ed. 59 (18) (2020) 7069–7075.
[21] J. Karges, F. Heinemann, M. Jakubaszek, F. Maschietto, C. Subecz, M. Dotou, R. Vinck, O. Blacque, M. Tharaud, B. Goud, E. Viñuelas Zahínos, B. Spingler, I. Ciofini, G. Gasser, Rationally Designed Long-Wavelength Absorbing Ru(II) Polypyridyl Complexes as Photosensitizers for Photodynamic Therapy, J. Am. Chem. Soc. 142 (14) (2020) 6578–6587.
[22] L. Conti, S. Ciambellotti, G.E. Giacomazzo, V. Ghini, L. Cosottini, E. Puliti, M. Severi, E. Fratini, F. Cencetti, P. Bruni, B. Valtancoli, C. Giorgi, P. Turano, Ferritin nanocomposites for the selective delivery of photosensitizing ruthenium-polypyridyl compounds to cancer cells, Inorgan. Chem. Front. 9 (6) (2022) 1070–1081.
[23] F. Li, E.J. Harry, A.L. Bottomley, M.D. Edstein, G.W. Birrell, C.E. Woodward, F. R. Keene, J.G. Collins, Dinuclear ruthenium(ii) antimicrobial agents that selectively target polysomes in vivo, Chem. Sci. 5 (2) (2014) 685–693.
[24] F. Li, M. Feterl, Y. Mulyana, J.M. Warner, J.G. Collins, F.R. Keene, In vitro susceptibility and cellular uptake for a new class of antimicrobial agents: dinuclear ruthenium(II) complexes, J. Antimicrob. Chemother. 67 (11) (2012) 2686–2695.
[25] F. Li, Y. Mulyana, M. Feterl, J.M. Warner, J.G. Collins, F.R. Keene, The antimicrobial activity of inert oligonuclear polypyridylruthenium(ii) complexes against pathogenic bacteria, including MRSA, Dalton Trans. 40 (18) (2011) 5032–5038.
[26] F.E. Poynton, S.A. Bright, S. Blasco, D.C. Williams, J.M. Kelly, T. Gunnlaugsson, The development of ruthenium(ii) polypyridyl complexes and conjugates for in vitro cellular and in vivo applications, Chem. Soc. Rev. 46 (24) (2017) 7706–7756.
[27] X.Y. Ng, K.W. Fong, L.V. Kiew, P.Y. Chung, Y.K. Liew, N. Delsuc, M. Zulkefeli, M. L. Low, Ruthenium(II) polypyridyl complexes as emerging photosensitisers for antibacterial photodynamic therapy, J. Inorg. Biochem. 250 (2024) 112425.
[28] L.-I. Rylands, A. Welsh, K. Maepa, T. Stringer, D. Taylor, K. Chibale, G.S. Smith, Structure-activity relationship studies of antiplasmodial cyclometallated ruthenium (II), rhodium (III) and iridium (III) complexes of 2-phenylbenzimidazoles, Eur. J. Med. Chem. 161 (2019) 11–21.
[29] N. Baartzes, A. Jordaan, D.F. Warner, J. Combrinck, D. Taylor, K. Chibale, G. S. Smith, Antimicrobial evaluation of neutral and cationic iridium(III) and rhodium (III) aminoquinoline-benzimidazole hybrid complexes, Eur. J. Med. Chem. 206 (2020) 112694.
[30] J. Yellol, S.A. Pérez, G. Yellol, J. Zajac, A. Donaire, G. Vigueras, V. Novohradsky, C. Janiak, V. Brabec, J. Ruiz, Highly potent extranuclear-targeted luminescent iridium(iii) antitumor agents containing benzimidazole-based ligands with a handle for functionalization, Chem. Commun. 52 (2016) 14165–14168.
[31] G.S. Yellol, A. Donaire, J.G. Yellol, V. Vasylyeva, C. Janiak, J. Ruiz, On the antitumor properties of novel cyclometalated benzimidazole Ru(ii), Ir(iii) and Rh (iii) complexes, Chem. Commun. 49 (2013) 11533–11535.
[32] B. Liu, S. Monro, M.A. Jabed, C.G. Cameron, K.L. Colón, W. Xu, S. Kilina, S. A. McFarland, W. Sun, Neutral iridium(iii) complexes bearing BODIPY-substituted N-heterocyclic carbene (NHC) ligands: synthesis, photophysics, in vitro theranostic photodynamic therapy, and antimicrobial activity, Photochem. Photobiol. Sci. 18 (10) (2019) 2381–2396.
[33] M. Lari, M. Martínez-Alonso, N. Busto, B.R. Manzano, A.M. Rodríguez, M.I. Acuña, F. Domínguez, J.L. Albasanz, J.M. Leal, G. Espino, B. García, Strong Influence of Ancillary Ligands Containing Benzothiazole or Benzimidazole Rings on Cytotoxicity and Photoactivation of Ru(II) Arene Complexes, Inorg. Chem. 57 (22) (2018) 14322–14336.
[34] P. Sen, N. Nwahara, T. Nyokong, Photodynamic antimicrobial activity of benzimidazole substituted phthalocyanine when conjugated to Nitrogen Doped Graphene Quantum Dots against Staphylococcus aureus, Main Group Chem. 20 (2021) 175–191.

[35] S. Swavey, A. Wertz, J. Erb, Bichromophoric Properties of Ruthenium(II) Polypyridyl Complexes Bridged by Boron Dipyrromethenes: Synthesis, Electrochemical, Spectroscopic, Computational Evaluation, and Plasmid DNA Photoreactions, Eur. J. Inorg. Chem. 2019 (32) (2019) 3690–3698.
[36] S.A. Archer, A. Raza, F. Dröge, C. Robertson, A.J. Auty, D. Chekulaev, J. A. Weinstein, T. Keane, A.J.H.M. Meijer, J.W. Haycock, S. MacNeil, J.A. Thomas, A dinuclear ruthenium(ii) phototherapeutic that targets duplex and quadruplex DNA, Chem. Sci. 10 (12) (2019) 3502–3513.
[37] L. Zeng, S. Kuang, G. Li, C. Jin, L. Ji, H. Chao, A GSH-activatable ruthenium(ii)-azo photosensitizer for two-photon photodynamic therapy, Chem. Commun. 53 (12) (2017) 1977–1980.
[38] L. Conti, E. Macedi, C. Giorgi, B. Valtancoli, V. Fusi, Combination of light and Ru (II) polypyridyl complexes: Recent advances in the development of new anticancer drugs, Coord. Chem. Rev. 469 (2022) 214656.
[39] Z. Huang, A.P. King, J. Lovett, B. Lai, J.J. Woods, H.H. Harris, J.J. Wilson, Photochemistry and in vitro anticancer activity of Pt(iv)Re(i) conjugates, Chem. Commun. 57 (85) (2021) 11189–11192.
[40] X. Zeng, Y. Wang, J. Han, W. Sun, H.-J. Butt, X.-J. Liang, S. Wu, Fighting against Drug-Resistant Tumors using a Dual-Responsive Pt(IV)/Ru(II) Bimetallic Polymer, Adv. Mater. 32 (43) (2020) 2004766.
[41] A. Welsh, L. Rylands, V.B. Arion, S. Prince, G.S. Smith, Synthesis and antiproliferative activity of benzimidazole-based, trinuclear neutral cyclometallated and cationic, N^N-chelated ruthenium(ii) complexes, Dalton Trans. 49 (2020) 1143–1156.
[42] A. Welsh, M. Mbaba, S. Prince, G.S. Smith, Synthesis, molecular modeling and preliminary anticancer evaluation of 2-ferrocenylbenzimidazole metallofragments, J. Mol. Struct. 1246 (2021) 131122.
[43] N. Msimango, A. Welsh, S. Prince, G.S. Smith, Synthesis and anticancer evaluation of trinuclear N^N quinolyl-benzimidazole-based PGM complexes, Inorg. Chem. Commun. 144 (2022) 109840.
[44] S. Fery-Forgues, D. Lavabre, Are Fluorescence Quantum Yields So Tricky to Measure? A Demonstration Using Familiar Stationery Products, J. Chem. Educ. 76 (9) (1999) 1260.
[45] A. Ogunsipe, J.-Y. Chen, T. Nyokong, Photophysical and photochemical studies of zinc(ii) phthalocyanine derivatives—effects of substituents and solvents, New J. Chem. 28 (7) (2004) 822–827.
[46] K. Suzuki, A. Kobayashi, S. Kaneko, K. Takehira, T. Yoshihara, H. Ishida, Y. Shiina, S. Oishi, S. Tobita, Reevaluation of absolute luminescence quantum yields of standard solutions using a spectrometer with an integrating sphere and a back-thinned CCD detector, Phys. Chem. Chem. Phys. 11 (42) (2009) 9850–9860.
[47] W. Spiller, H. Kliesch, D. Wöhrle, S. Hackbarth, B. Röder, G. Schnurpfeil, Singlet oxygen quantum yields of different photosensitizers in polar solvents and micellar solutions, J. Porphyrins Phthalocyanines 2 (2) (1998) 145–158.
[48] A.M. Potocny, J.J. Teesdale, A. Marangoz, G.P.A. Yap, J. Rosenthal, Spectroscopic and 1O2 Sensitization Characteristics of a Series of Isomeric Re(bpy)(CO)3Cl Complexes Bearing Pendant BODIPY Chromophores, Inorg. Chem. 58 (8) (2019) 5042–5050.
[49] E.T. Papish, O.E. Oladipupo, Factors that influence singlet oxygen formation vs. ligand substitution for light-activated ruthenium anticancer compounds, Curr. Opin. Chem. Biol. 68 (2022) 102143.
[50] C. Kreitner, K. Heinze, Excited state decay of cyclometalated polypyridine ruthenium complexes: insight from theory and experiment, Dalton Trans. 45 (35) (2016) 13631–13647.
[51] L.D. Ramos, H.M. da Cruz, K.P. Morelli Frin, Photophysical properties of rhenium (i) complexes and photosensitized generation of singlet oxygen, Photochem. Photobiol. Sci. 16 (4) (2017) 459–466.
[52] S. Doose, H. Neuweiler, M. Sauer, Fluorescence Quenching by Photoinduced Electron Transfer: A Reporter for Conformational Dynamics of Macromolecules, Chem. Phys. Chem. 10 (9-10) (2009) 1389–1398.
[53] H.N. Akl, D. Salah, H.S. Abdel-Samad, A.A. Abdel Aziz, A.A. Abdel-Shafi, Fractional dependence of the free energy of activation on the driving force of charge transfer in the quenching of the excited states of substituted phenanthroline homoleptic ruthenium(ii) complexes in aqueous medium, RSC Adv. 13 (19) (2023) 13314–13323.
[54] S.A. McFarland, A. Mandel, R. Dumoulin-White, G. Gasser, Metal-based photosensitizers for photodynamic therapy: the future of multimodal oncology? Curr. Opin. Chem. Biol. 56 (2020) 23–27.
[55] N.U. Prajith, P.V. Priyanka, V. Alexander, Synthesis, characterization, photophysical, lipophilicity, and in vitro fluorescence studies of mono-, di-, and trinuclear Ru(II) polypyridyl complexes of pyridinyl benzimidazole derivatives, J. Biol. Inorg. Chem. 27 (3) (2022) 357–372.
[56] L. Conti, E. Macedi, C. Giorgi, B. Valtancoli, V. Fusi, Combination of light and Ru (II) polypyridyl complexes: Recent advances in the development of new anticancer drugs, Coord. Chem. Rev. 469 (2022) 214656.
[57] J. Liu, C. Zhang, T.W. Rees, L. Ke, L. Ji, H. Chao, Harnessing ruthenium(II) as photodynamic agents: Encouraging advances in cancer therapy, Coord. Chem. Rev. 363 (2018) 17–28.
[58] J. Karges, S. Kuang, F. Maschietto, O. Blacque, I. Ciofini, H. Chao, G. Gasser, Rationally designed ruthenium complexes for 1- and 2-photon photodynamic therapy, Nat. Commun. 11 (1) (2020) 3262.
[59] I. Koyuncu, Y. Tülüce, H. Slahaddin Qadir, M. Durgun, C.T. Supuran, Evaluation of the anticancer potential of a sulphonamide carbonic anhydrase IX inhibitor on cervical cancer cells, J. Enzyme Inhib. Med. Chem. 34 (1) (2019) 703–711.
[60] H.E. Hashem, A.E.-G.E. Amr, E.S. Nossier, M.M. Anwar, E.M. Azmy, New Benzimidazole-, 1,2,4-Triazole-, and 1,3,5-Triazine-Based Derivatives as Potential EGFRWT and EGFRT790M Inhibitors: Microwave-Assisted Synthesis, Anticancer Evaluation, and Molecular Docking Study, ACS Omega 7 (8) (2022) 7155–7171.
[61] S. Cascioferro, B. Parrino, V. Spanò, A. Carbone, A. Montalbano, P. Barraja, P. Diana, G. Cirrincione, 1,3,5-Triazines: A promising scaffold for anticancer drugs development, Eur. J. Med. Chem. 142 (2017) 523–549.
[62] R. Satrialdi, V. Munechika, Y. Biju, H. Takano, Y. Harashima, Yamada, The optimization of cancer photodynamic therapy by utilization of a pi-extended porphyrin-type photosensitizer in combination with MITO-Porter, Chem. Commun. 56 (7) (2020) 1145–1148.
[63] L. Wang, H. Yin, M.A. Jabed, M. Hetu, C. Wang, S. Monro, X. Zhu, S. Kilina, S. A. McFarland, W. Sun, π-Expansive Heteroleptic Ruthenium(II) Complexes as Reverse Saturable Absorbers and Photosensitizers for Photodynamic Therapy, Inorg. Chem. 56 (6) (2017) 3245–3259.
[64] L.K. McKenzie, H.E. Bryant, J.A. Weinstein, Transition metal complexes as photosensitisers in one- and two-photon photodynamic therapy, Coord. Chem. Rev. 379 (2019) 2–29.
[65] R. Matshitse, N. Nwaji, M. Mananga, E. Prinsloo, T. Nyokong, Effect of number of positive charges on the photophysical and photodynamic therapy activities of quarternary benzothiazole substituted zinc phthalocyanine, J. Photochem. Photobiol. A Chem. 367 (2018) 253–260.
[66] H. Tokunaga, T. Nakanishi, T. Iwata, D. Aoki, T. Saito, S. Nagase, F. Takahashi, N. Yaegashi, Y. Watanabe, Effects of chemotherapy on patients with recurrent cervical cancer previously treated with concurrent chemoradiotherapy: a retrospective multicenter survey in Japan, Int. J. Clin. Oncol. 20 (3) (2015) 561–565.
[67] H.J. Long, Management of Metastatic Cervical Cancer: Review of the Literature, J. Clin. Oncol. 25 (20) (2007) 2966–2974.
[68] Y. Zhang, X. Zhang, H. Zhu, Y. Liu, J. Cao, D. Li, B. Ding, W. Yan, H. Jin, S. Wang, Identification of Potential Prognostic Long Non-Coding RNA Biomarkers for Predicting Recurrence in Patients with Cervical Cancer, Cancer Manag. Res. 12 (2020) 719–730.
[69] H. Zhu, H. Luo, W. Zhang, Z. Shen, X. Hu, X. Zhu, Molecular mechanisms of cisplatin resistance in cervical cancer, Drug. Des. Devel. Ther. 10 (2016) 1885–1895.
[70] E. Delaey, F. van Laar, D. De Vos, A. Kamuhabwa, P. Jacobs, P. de Witte, A comparative study of the photosensitizing characteristics of some cyanine dyes, J. Photochem. Photobiol. B Biol. 55 (1) (2000) 27–36.
[71] A. Frei, R. Rubbiani, S. Tubafard, O. Blacque, P. Anstaett, A. Felgenträger, T. Maisch, L. Spiccia, G. Gasser, Synthesis, Characterization, and Biological Evaluation of New Ru(II) Polypyridyl Photosensitizers for Photodynamic Therapy, J. Med. Chem. 57 (17) (2014) 7280–7292.
[72] N.M. Motimani, S. Ngubane, G.S. Smith, Polynuclear heteroleptic ruthenium(II) photoredox catalysts: Evaluation in blue-light-mediated, regioselective thiol-ene reactions, Polyhedron 212 (2022) 115616.
[73] M.D. Hossain, M.-A. Haga, B. Gholamkhass, K. Nozaki, M. Tsushima, N. Ikeda, T. Ohno, Syntheses, Spectroelectrochemistry and Photoinduced Electron-Transfer Processes of Novel Ru and Os Dyad and Triad Complexes with Functionalized Diimide Ligands, Collect. Czechoslov. Chem. Commun. 66 (2) (2001) 307–337.
[74] M. Ishiyama, H. Tominaga, M. Shiga, K. Sasamoto, Y. Ohkura, K. Ueno, A Combined Assay of Cell Viability and in Vitro Cytotoxicity with a Highly Water-Soluble Tetrazolium Salt, Neutral Red and Crystal Violet, Biol. Pharm. Bull. 19 (11) (1996) 1518–1520.
[75] M. Oparka, J. Walczak, D. Malinska, L.M.P.E. van Oppen, J. Szczepanowska, W.J. H. Koopman, M.R. Wieckowski, Quantifying ROS levels using CM-H2DCFDA and HyPer, Methods 109 (2016) 3–11.
[76] S. Kimani, S. Chakraborty, I. Irene, J. de la Mare, A. Edkins, A. du Toit, B. Loos, A. Blanckenberg, A. Van Niekerk, L.V. Costa-Lotufo, K.N. ArulJothi, S. Mapolie, S. Prince, The palladacycle, BTC2, exhibits anti-breast cancer and breast cancer stem cell activity, Biochem. Pharmacol. 190 (2021) 114598.